Enhancing TiO₂ activity for CO₂ photoreduction through MgO decoration

Juliana A. Torres, ^a André E. Nogueira, ^b Gelson T. S. T. da Silva, ^{ac} Osmando F. Lopes, ^d
Yanjie Wang, ^e Tao He, ^{ef} and Caue Ribeiro, ^{ag*}

^aNational Nanotechnology Laboratory for Agribusiness (LNNA), Embrapa Instrumentation, 13561-206, São Carlos – SP, Brazil.

^bDepartment of Chemistry, Institute of Exact and Biological Sciences (ICEB), Federal University of Ouro Preto (UFOP), 35400-000, Ouro Preto – Minas Gerais, Brazil.
^cDepartment of Chemistry, Federal University of São Carlos (UFSCar), 13565-905, São Carlos – São Paulo, Brazil.

^dInstitute of Chemistry, Federal University of Uberlândia (IQUFU), 38400-902, Uberlândia – Minas Gerais, Brazil.

^eCAS Key Laboratory of Nanosystem and Hierarchical Fabrication, CAS Center for Excellence in Nanoscience, National Center for Nanoscience and Technology, Beijing 100190, China.

^fUniversity of Chinese Academy of Sciences, Beijing 100049, China.
^gForschungszentrum Jülich GmbH – Institut of Energy and Climate Research – IEK3/Electrochemical Process Engineering, Jülich 52425, Germany.
E-mail: caue.ribeiro@embrapa.br.

Herein we report on the influence of MgO's basic character in the photoactivity of MgO:TiO₂ nanocomposites for the CO₂ reduction reaction. TiO₂ nanoparticles, decorated with MgO in different mass proportions, were synthesized by the physical mixing of pre-synthesized oxides followed by calcination. The decorated samples presented enhanced photocatalytic activity with higher selectivity for CO, while CH₄ was also produced, as well as HCOOH and CH₃COOH in a liquid medium in lower proportions. The results indicate that the beneficial MgO influence is only effective at low amounts, whilst a high MgO amount favors an insulating behavior instead of semiconducting, reducing the nanocomposite performance for CO₂ photoreduction.

Keywords: CO_2 photoreduction; Artificial photosynthesis; Basic metal oxides; TiO_2/MgO .

1. Introduction

The increase in carbon dioxide (CO₂) concentration in the atmosphere is directly causal in the greenhouse effect and strategies are constantly being developed to reduce its emission [1-4]. Amongst these, conversion to other useful chemicals and products

(CH₄, CO, CH₃COOH, CH₃OH, amongst others) is highly promising. Photocatalytic CO₂ reduction has the potential of solar light-driven process, which is advantageous in terms of energy balance [4,5,16,17], but this technology still faces challenges related to the low adsorption of CO₂ molecules, semiconductor surfaces, limited desorption of the intermediates and reaction products, the fast recombination rate of the photogenerated pairs (*e*⁻/h⁺), as well as low performance of the used catalysts [6,7,15].

Of the various proposed semiconductors, TiO₂ is still the most studied considering its low cost, high availability, stability and non-toxic nature, aside from it being easily synthesized [8,9]. However, this oxide still has limited photocatalytic efficiency for reduction, mainly due to weak binding with CO₂. The addition of basic metal oxides, particularly MgO, considerably increases the adsorption capacity of CO₂ molecules on the TiO₂ surface [8,10-12], as CO₂ is a Lewis acid. Thus, CO₂ might be adsorbed into an MgO layer over TiO₂ to become destabilized and, consequently, more active than CO₂ in its linear form [3,13]. However, on the other hand, MgO interaction to CO₂ tends to form stable MgCO₃, which in large amounts could poison the surface and therefore limit the TiO₂ activity [14]. Comparing the available literature, there is no consensus about how MgO is beneficial to this reaction and in which contents the catalytical activity is properly enhanced.

Therefore, we have shown that the addition of MgO on the TiO₂ surface can improve the efficiency of CO₂ photoreduction in aqueous media driven by its basic surface, but this effect is only positive with small MgO amounts, supporting the notion that TiO₂/MgO nanocomposites are plausible candidates for the photoreduction process. To that, we propose a synthetic path based on the coalescence of previously formed nanoparticles through the hydrothermal synthesis of TiO₂-elongated nanoparticles and the calcination route for MgO. The use of pre-formed oxides minimized the risk of unintentional doping or titanate production that could interfere with the analysis of the actual MgO role over TiO₂.

2. Experimental

2.1 Synthesis

MgO was obtained by annealing treatment of the MgO(NO₃)₂.6H₂O (Synth/P.A.) at 500 °C for 2 h with a heating rate of 3 °C min⁻¹. TiO₂ nanorices were obtained using a two-step hydrothermal method. In the first step, TiO₂ P25 (Degussa) was dispersed in alkaline solution of NaOH (10 mol L⁻¹), placing the capsule in an autoclave, while the

hydrothermal treatment was performed at 140 °C for 24 h. Thereafter, the produced sodium titanate was subjected to a second hydrothermal process at 200 °C for 12 h. Finally, the produced TiO₂ nanorices were centrifuged, washed and dried at 50 °C overnight. For the synthesis of the TiO₂/MgO nanocomposite, the two oxides previously obtained were mixed in different mass proportions of 1.0, 2.0 and 5.0% (w/w) and then calcined at 150 °C for 2 h at a heating rate of 3 °C min⁻¹, which were referred to as TiO₂/MgO 1%, TiO₂/MgO 2% and TiO₂/MgO 5%, respectively.

2.2 Characterization

The morphology of the samples was obtained by field emission gun scanning electron microscopy (FEGSEM) JEOL JSM 6701F. The crystalline phase of TiO₂ and nanocomposites powder were characterized by X-ray diffraction (XRD) using CuKα radiation in the 2θ range from 20 to 80°, employing a Shimadzu XRD-6000 diffractometer. Raman measurements were obtained with an FT-Raman spectrometer (Bruker RAM II with a Ge detector) equipped with an Nd:YAG. All spectra were acquired at an excitation wavelength of 1064 nm, generating a power of 100 mW at a resolution of 2 cm⁻¹. The formation of nanocomposites was verified using high resolution transmission electron microscopy (HRTEM) employing the TECNAI G2 F20 microscope (FEI), operated at 200 kV. Colloid suspensions were dripped onto wetting carbon-coated copper grids and then dried in the air to obtain the images. The microscopy integrated with X-ray energy-dispersive spectroscopy (XEDS) was also employed for elementary characterization of the nanocomposite containing 1% magnesium (TiO₂/MgO 1%). Diffuse reflectance spectra (DRS) in the ultraviolet-visible region were recorded between 200 and 800 nm, at room temperature, using a Cary 5G instrument (Varian) operated in diffuse reflectance mode to determine the band gap of the materials. The zeta potentials of the TiO₂/MgO 1% nanocomposite and TiO₂ pure were determined with a Zeta Sizer nano-ZS instrument (Malvern Instruments) in the pH range from 9 to 2, with the pH adjusted by adding 0.1 mol L-1 HCl or 0.1 mol L-1 NaOH. The surface composition and elemental chemical state of the co-obtained sample were investigated by X-ray photoelectron spectroscopy (XPS) using a K-Alpha XPS instrument (Thermo Fisher Scientific, UK). The incident radiation used was Al Ka Xrays, >10⁻⁸ mbar of vacuum, and with charge compensation during the measurements. Surveys and high-resolution spectra were recorded using a pass energy of 1 eV, with 5 scans and 0.1 eV with 50 scans, respectively. The binding energy was referenced to the

C 1s peak at 284.7 eV. A data analysis was performed using Casa XPS software. The specific surface area values were calculated using the Brunauer-Emmett-Teller (BET) method and pore size distribution were determined from the adsorption branch of the isotherm using the Barrett-Joyner-Halenda (BJH) method. Samples were previously degassed at 80 °C under vacuum until a degassing pressure <10 µmHg and N₂ adsorption-desorption isotherms were measured with a Micromeritics ASAP 2020 analyzer at 77 K. Diffuse reflectance infrared Fourier transform spectroscopy (DRIFTS) for in situ adsorption of carbon dioxide (CO₂) were obtained in a Thermo Nicolet 4700 Nexus FT-IR Spectrophotometer with MCT-B Detector (Mercury Teluride Cadmium) using a DRIFTS cell from Harrick Scientific with a CaF₂ window. The spectra were collected with 30 scans and 4 cm⁻¹ resolution. Initially, samples were pretreated with a flow of 40 mL min⁻¹ N₂ for 30 minutes at 25 °C. Then, the *in situ* adsorption step was commenced with a flow of 15 mL min⁻¹ of CO₂ at 25 °C collecting spectra every 1 minute. After complete saturation of the medium with CO₂, the desorption of the species was carried out with 40 mL min⁻¹ of N₂ at room temperature until the signal stabilized, collecting the spectra every 1 minute up to 5 minutes.

2.3 CO₂ photoreduction

The CO₂ photoreduction reaction occurred in a 225 mL-capacity cylindrical steel reactor, covered with borosilicate glass under UVC light (PHILIPS 5W), with a maximum wavelength of 253.7 nm (0.167 mW/cm²) (Fig. S1). Samples of 100 mg of the nanocomposites or pure TiO₂ were dispersed in 100 mL of distilled water or in 100 mL of NaOH (0.1 mol L⁻¹) solution that was constantly stirred. Before starting the reaction, high-purity CO₂ gas was bubbled for 20 min to saturate the reactor and ensure that all the oxygen had been eliminated.

The reactor used in photoreduction is surrounded by a heat exchanger so that it allows temperature control that was kept constant at 25 °C throughout the reaction period. Since the solubility of a gas is temperature dependent, where at high temperatures they have reduced solubility [18], this setup was chosen to keep reactions at low temperatures ensuring higher CO₂ solubility in water.

At determined time intervals, aliquots of 200 μ L of the gas phase were collected and analyzed to evaluate the progress of the reaction. For this, a gas chromatograph (model CP-3800, Varian) equipped with a thermal conductivity detector (TCD) and flame ionization detector (FID), as well as a packed column (HayeSep N (0.5 m x 1.8")) was

used. The gas flow rates were 30 mL min⁻¹ for H₂, 300 mL min⁻¹ for air and 30 mL min⁻¹ for N₂. The injector temperature was 150 °C, 200 °C for the TCD detector and 150 °C for the FID detector. The quantification of products and yield of the reactions was calculated using injections of standard gaseous mixtures.

To evaluate the products formed in the liquid phase, high performance liquid chromatography (HPLC-LC-20AD, Shimadzu) was used. After 24 h of reaction, aliquots of 20 μL were injected into an Aminex HPX-87H column (300 x 7.8 mm) and kept at a constant temperature of 40 °C capable of analyzing carboxylic acids and alcohols, in dilute H₂SO₄ solution (0.33 mmol L⁻¹) as a mobile phase at 0.6 mL min⁻¹. The experiment of CO₂ reduction over 48 h was performed with the TiO₂/MgO 1% nanocomposite and aliquots were withdrawn for the liquid phase analysis over this period. This chromatograph is equipped with a differential refractive index detector (RID-10A) suitable for alcohols, while a UV-Vis detector (SPD-20A, 210 nm) with deuterium lamp suitable for carboxylic acids.

3. Results and discussion

3.1 Characterization of samples

The morphological characteristics of the isolated semiconductors (MgO and TiO₂) and nanocomposites are shown in Fig. 1, and for comparison purposes, the morphology of Na₂TiO₃ (the precursor to TiO₂) can also be seen (Fig. S2). The Na₂TiO₃ obtained in the first hydrothermal treatment step has an undefined shape (Fig. S2a), whereas after the second hydrothermal treatment, the TiO₂ nanorices are clearly observed (Fig. 1a). MgO, on the other hand, shows agglomerated micrometric particles (Fig. S2b), with some denser regions. After the physical mixing and calcination of TiO₂ with MgO at different mass ratios, a slight change in TiO₂ nanorices morphology can be observed (Fig. 1b-d). These materials exhibit similar morphologies to pristine TiO₂, but with some irregular particles on its surface attributed to MgO.

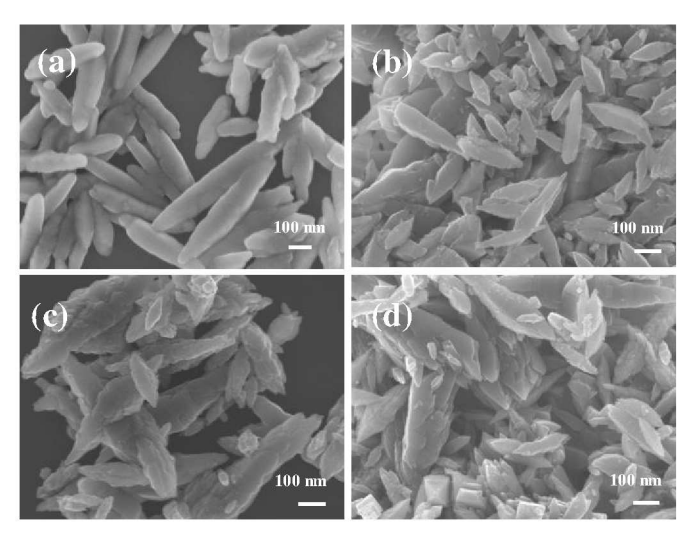


Fig. 1 SEM images of the TiO_2 (a) and TiO_2/MgO prepared at different mass proportions; (b) TiO_2/MgO 1%; (c) TiO_2/MgO 2%; and (d) TiO_2/MgO 5%.

Fig. 2 shows the XRD patterns of pure TiO₂ and MgO, as well as the different composition of MgO on TiO₂. The anatase TiO₂ planes are observed in the XRD

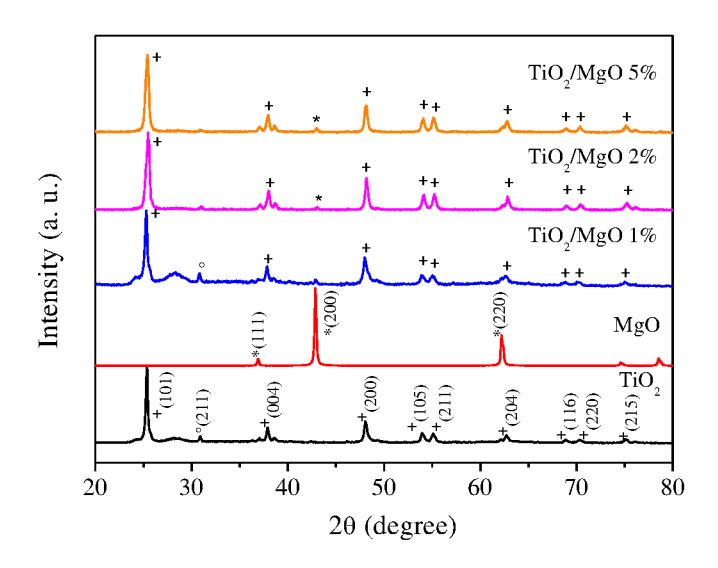


Fig. 2 Full XRD patterns for TiO₂, MgO and nanocomposites obtained by the physical mixing of the respective oxides at 1, 2 and 5% of MgO (*Anatase TiO₂; Brookite TiO₂ and *MgO periclase).

patterns, as is a characteristic peak of the brookite phase that was identified at 30.9° in the synthesized TiO_2 and relates to the plane (211) [JCPDS #75-1582] [19]. The nanocomposites containing 1, 2 and 5% of MgO exhibit diffraction peaks corresponding to the tetragonal anatase phase of TiO_2 , with Bragg diffraction at $2\theta = 25.3^{\circ}$, 37.9° , 48.1° , 53.9° , 55.0° , 62.7° , 68.8° , 70.3° and 75.1° , respectively, assigning to the diffraction planes (101), (004), (112), (200), (105), (211), (204), (116), (220) and (215), in agreement with the standard data. In the nanocomposite containing, 1% of MgO, it was not possible to observe any change in TiO_2 crystalline phase, probably due to the high dispersion and low MgO content on the TiO_2 surface [20, 21]. However, at higher loadings of MgO (i.e., TiO_2/MgO 2% and TiO_2/MgO 5%), a new peak at 42.8° is observed, referring to the cubic MgO periclase phase [JCPDS #87-0653] [22].

Raman spectroscopy was used as an additional technique to X-ray diffraction to confirm the medium-range structure. The spectra evolution for the different samples are shown in the Fig. 3a, the enlarged spectrum of the region from 500 cm⁻¹ to 150 cm⁻¹ can be verified at Fig. 3b. Synthesized TiO₂ shows essentially four peaks, being 144 cm⁻¹, 399 cm⁻¹, 515 cm⁻¹ and 639 cm⁻¹, attributed to E_g, B_{1g}, A_{1g} and E_g active vibrations of

anatase TiO₂, respectively [14,23]. All of the nanocomposites showed characteristic peaks of the TiO₂ anatase phase, as well as peculiar peaks to the brookite phase shown in the enlarged spectrum, which corroborates the data collected in X-ray diffraction, indicating that brookite and anatase phases were obtained under the synthesis conditions used. Despite the well-known performance of the TiO₂ anatase phase in photocatalytic reactions, the presence of the brookite phase plays an important role in the semiconductor performance, considering the synergistic effect between these two phases, which can improve the efficiency of the reactions [14]. For the brookite phase, six active vibrations in the enlarged Raman spectrum were identified at 214 cm⁻¹ (B_{1g}), 247 cm⁻¹ (A_{1g}), 287 cm⁻¹ (B_{1g}), 322 cm⁻¹ (B_{1g}), 366 cm⁻¹ (B_{2g}) and 452 cm⁻¹ (B_{2g}). However, when MgO content increases to 2 and 5%, the brookite TiO₂ changes to anatase, probably by surface diffusion. As the transformation brookite to anatase is topotactic, small surface modifications can easily induce transformation to the most stable phase [14,19,24].

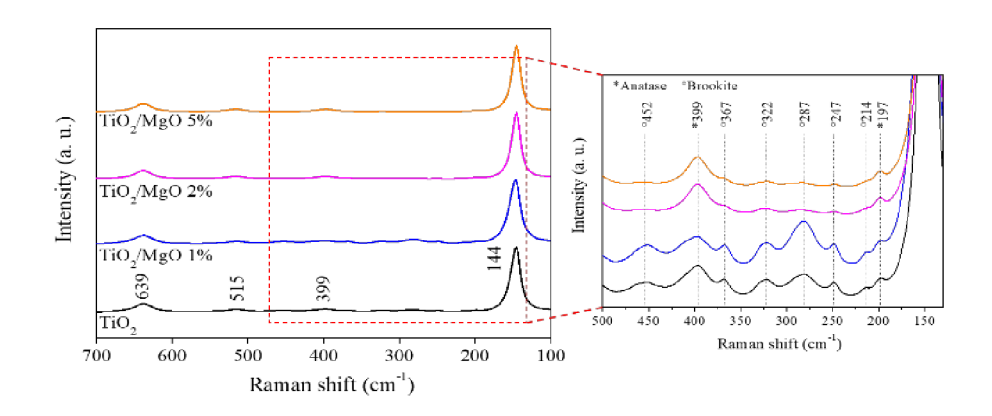


Fig. 3 Full and enlarged Raman spectra for TiO₂, MgO and nanocomposites obtained by the physical mixing of the respective oxides at 1, 2 and 5% of MgO.

In order to study the TiO₂/MgO 1% microstructure in detail, HRTEM and the element mapping analyses were performed (Fig. 4). The HRTEM image shows a TiO₂ anatase phase in the nanocomposite with 0.35 nm interplanar spacing, corresponding to the (101) plane [8,21]. It is possible to confirm the presence of MgO particles on the TiO₂ surface, with an interplanar spacing of the 0.21 nm ((200) plane), indicating the formation of nanocomposite between these two oxides [13,21]. Other evidence of the presence of MgO on the surface of TiO₂ was obtained from the elemental X-ray

mapping results. These results suggest that the Mg species are evenly dispersed on the TiO₂ surface (Fig. 4c).

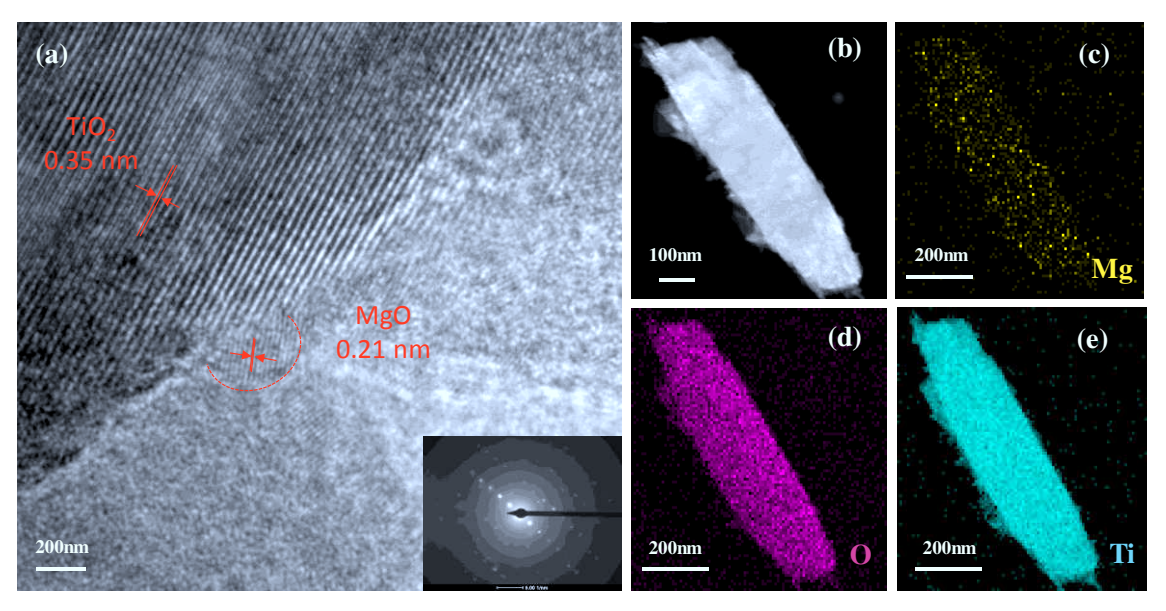


Fig. 4 HRTEM image (a) and mapping of the TiO₂/MgO 1% calcined at 150 °C; (b) TEM; (c) Mg mapping; (d) O mapping; and (e) Ti mapping.

The determination of the optical properties of photocatalysts is closely related to their efficiency in photocatalytic reactions. Thus, these properties were determined for all samples obtained using UV-vis diffuse reflectance spectroscopy (UV-vis DRS). Absorption edges (*Eg*) were determined by means of the Tauc method (Fig. S3) [25,26]. The absorption edge was identical between the TiO₂ semiconductor and the nanocomposites containing 1 and 2% MgO (3.3 eV), whereas for the nanocomposite containing 5%, the value identified was close to 3.4 eV. These results suggest that smaller MgO additions do not significantly interfere in photoactivation (as the absorption edge is similar to the TiO₂ band gap), but in higher contents (i.e., 5%) modify the optical property, shifting to more insulating behavior, which can be deleterious for the photocatalytic activity of the nanocomposites. Considering the MgO contents, this effect is probably associated with the oxide coverage, leading to a fully covered TiO₂.

An XPS analysis was performed to investigate the surface composition and chemical state of the elements in TiO₂/MgO 1%, TiO₂ and the MgO as-obtained samples, as can be seen in Fig. 5. From the survey spectra for the TiO₂/MgO 1% sample (Fig. 5a), Ti, Mg, O and C (this was used as an internal reference) were confirmed, without the presence of any contamination. The high-resolution spectra of the Ti 2p region for the TiO₂ sample pristine exhibited two characteristic peaks around 458.3 eV and 464.0 eV, which are indexed to Ti 2p_{3/2} and Ti 2p_{1/2}, respectively. On other hand, the TiO₂/MgO 1% nanocomposite exhibited a positive shift in these peaks for 458.7 eV and 464.5 eV, which is indicative of the heterojunction formation, as it is expected that the interaction between the phases changes the chemical environmental. The high-resolution spectra of the region of O1s for pristine TiO₂ exhibit a wide and slightly asymmetrical peak, indicating that other oxygen species are present in the surface region, and that these oxygen species might be hydroxyl oxygen and adsorbed oxygen on the surface of the as-obtained samples. TiO2/MgO 1% nanocomposite exhibits a small positive shift in these peaks. On the other hand, the MgO sample exhibits a more symmetrical peak with strong positive shift [21,27-29]. Finally, in the Mg 1s, high-resolution spectra confirm that MgO and TiO₂/MgO 1% exhibited the same profile, which is indicative that the method was efficient for the deposition of MgO on the TiO₂ samples, even at the low concentration. An estimation of the Mg content by XPS data (by peak integration) indicates a molar relationship of 0.116 Mg/Ti, higher than what was expected by the synthesis stoichiometry (0.02 Mg/Ti). As XPS is more sensitive to surface atoms, this result indicates that MgO was not incorporated but actually dispersed over the TiO₂ surface.

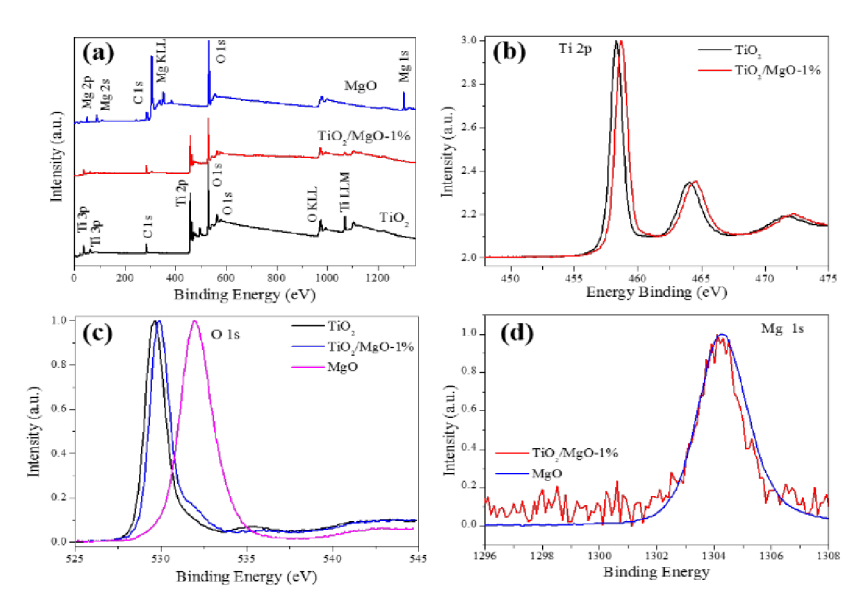


Fig. 5 (a) Survey spectra and high-resolution spectra of the (b) Ti 2p region; (c) O 1s region; (d) Mg 1s region of the samples as obtained.

The textural properties of the samples were evaluated by N₂ adsorption-desorption and all materials presented a higher amount of mesopores, and as expected, the surface area decreased slightly after the MgO addition to the TiO₂ surface, from 23 m² g⁻¹ for pure TiO₂ to 15 m² g⁻¹ for MgO-decorated samples. Thus, it is attributed to the improved adsorption of CO₂ molecules to the addition of MgO on the TiO₂ surface, rather than to the adsorption process, given the small surface area of the materials. However, the reduction in surface area indicates that the increase in photocatalytic activity for decorated samples is correct, not an artifact of different surface areas.

3.2 Photocatalytic performance of TiO_2 and nanocomposites in the CO_2 photoreduction

The photocatalytic performance of pure TiO_2 and TiO_2/MgO nanocomposites in water and NaOH basic solution (0.1M) are shown in Fig. 6. The maximum amount of methane produced during all the reactions of CO_2 photoreduction carried out in NaOH- solution were higher than those in the aqueous medium (Fig. 6b). This phenomenon can be explained by the higher solubility of CO_2 molecules in NaOH solution compared to pure water. In fact, before the photoreaction the NaOH solution had stabilized in pH = 6.74 (after 20 min of CO_2 bubbling), while the aqueous system had reached pH = 4.18,

indicating that the reaction in the NaOH system was carried on over HCO_3^- ions instead of soluble CO_2 . The local acidity also reveals the consumption of CO_2 during the reaction: after 6 hours, pH in an aqueous medium system rises to 4.61, while in the NaOH system it reaches 7.24. In both cases, the acidity is defined by the effective amount of CO_2 in the solution, with the rising pH indicating the extension of CO_2 photoconversion [10].

According to the fundamentals of photocatalysis, as a semiconductor is photoexcited by irradiation with energy equal to or greater than the band gap energy, an electron is transferred from the valence band (VB) to conduction band (CB), forming an electron-hole pair (e^-/h^+). Semiconductors with high valence band potential, as in the case of TiO₂ (E_{VB} 2.95 V vs. NHE) [16,17,30], have holes with high oxidizing power which, in our case, are involved in O₂ evolution from water. As in the case of the TiO₂/MgO samples presented in this manuscript, MgO acted mainly in the intensification of the CO₂ molecules adsorption process due to its basic character, while the reaction medium water molecules were oxidized in the valence band of TiO₂ (H₂O/O₂ +0.82V).

Aside from the difference in performance with respect to the reaction medium, it is

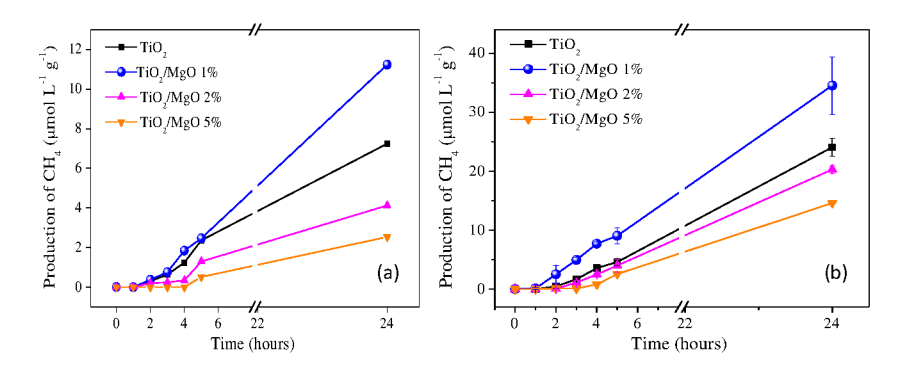


Fig. 6 Photocatalytic reduction of CO_2 to CH_4 in pure water (a) and in 0.1M NaOH solution (b) with the TiO_2 and nanocomposites with different proportions of MgO, 1, 2 and 5%.

observed that the nanocomposite containing 1% of MgO showed a higher production of CH₄ in relation to the other analyzed samples (Fig. 6b). We assume that, as CO₂ is likely to adsorb over MgO layer at TiO₂ surface, metastable magnesium carbonate species are formed [10]. However, with higher amounts of MgO (TiO₂/MgO 2% and 5%), the catalytic efficiency diminishes, suggesting that the insulating effect of the MgO particles prevails. As high amounts of MgO species can fully cover the TiO₂

surface, this can prevent the migration of the photogenerated charge carriers at the TiO_2 surface and thus leads to reduced activity [21].

In addition, some studies reveal that the adsorption of CO₂ in TiO₂/MgO-type nanocomposites may lead to the formation of bidentate carbonate (b-CO₃²⁻) and bicarbonates (HCO₃⁻), which is in accordance with our findings in *in situ* FTIR (Fig. 8). The generated HCO₃⁻ are possible intermediates for the formation of CO and C1 fuels, unlike the b-CO₃²⁻ species, which can accumulate on the surface of the catalysts, leading to a decrease in efficiency, which may also explain the reduction in methane production by the nanocomposites with higher MgO content [9] – as evinced by HRTEM and element mapping, MgO is uniformly distributed on the TiO₂ surface. A second product present in higher quantities in the CO₂ photoreduction compared to CH₄ was CO (Fig. 7), which corroborates the results obtained in previous studies [31]. However, for CO formation, no significant difference was observed amongst the samples. This indicates that the MgO content does not alter the CO formation pathway, and that the reduction process starts in any case at the TiO₂ surface [9].

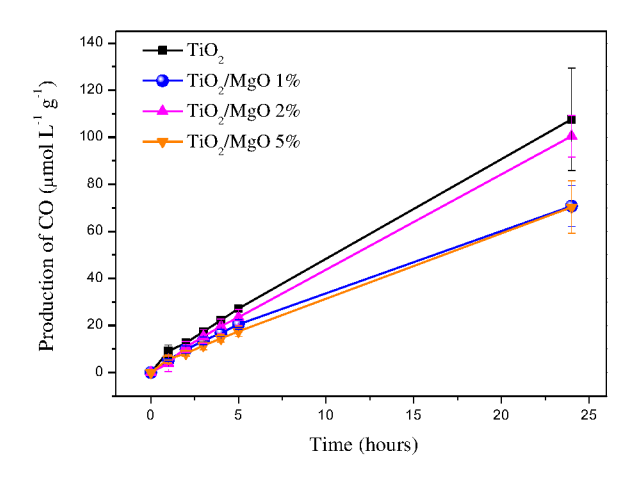


Fig. 7 Photocatalytic reduction of CO₂ to CO in 0.1M NaOH solution with the TiO₂ and nanocomposites with different proportions of MgO, 1, 2 and 5%.

Some authors suggest possible pathways based on the main products, CO, CH₄ and CH₃OH. CO, for example, may be formed from the decomposition of HCOOH by irradiation (HCOOH + $hv \rightarrow$ CO) [10]. With CH₄, in turn, although different pathways are proposed in the literature, the most cited is its synthesis, having the CO itself as an intermediate (CO + $e^- \rightarrow$ C' + H' \rightarrow CH₃' + H' \rightarrow CH₄) [10,31,32].

During the CO_2 photoreduction process, after physisorption of this molecule, numerous reactions with different intermediate compounds can be formed, depending on the semiconductor characteristics and reaction conditions. One of the ways proposed in the literature for CH_4 production, goes through CO as discussed. However, CH_4 can also be produced by reducing CO_2 , which requires eight electrons and eight protons $(CO_2 + 8H^+ + 8e^- \rightarrow CH_4 + 2H_2O)$. Therefore, CO reduction to CH_4 is thermodynamically and kinetically more favorable than the reduction of CO_2 for CH_4 [33-36]. Thus, the production of CH_4 may be related to both CO_2 adsorption on the semiconductor surface and the ability to reduce CO to CH_4 . The latter in turn needs CO adsorbed on the catalyst surface or the same solubilized in the aqueous medium.

Considering that for CO production only two protons and two electrons are required $(CO_2 + 2H^+ + 2e^- \rightarrow CO + H_2O)$, its formation is more favorable compared to CH_4 , which requires eight protons and eight electrons $(CO_2 + 8H^+ + 8e^- \rightarrow CH_4 + 2H_2O)$ [21]. Thus, it is inferred that the lower production of CH_4 compared to CO may be related to this condition, but is also influenced by the surface affinity for CO_2 , requiring higher electron transference. These results were confirmed in another photoreduction setup with similar trends in CO_2 photoreduction, despite the difference in relation to

reactor design and reaction conditions (as seen in Fig. S5). Fig. 8 shows a comparison of CH₄ and CO production by different samples.

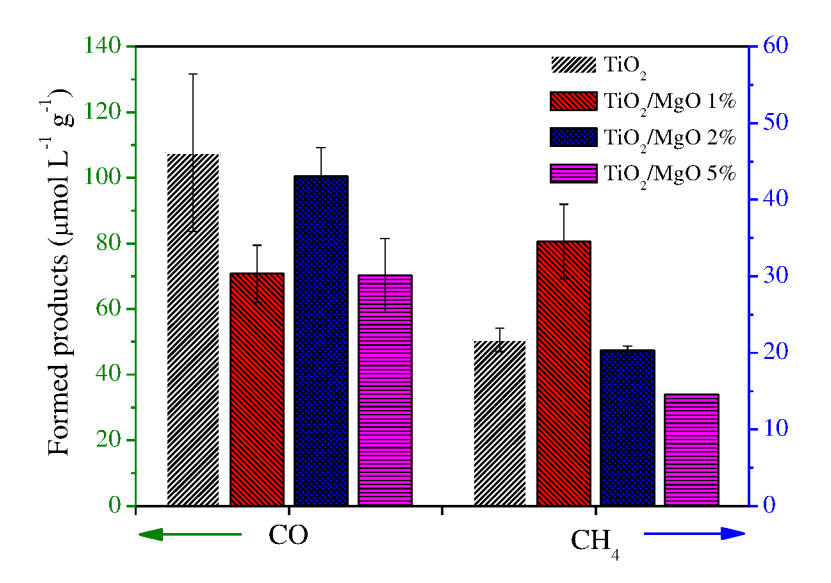


Fig. 8 Photocatalytic reduction of CO_2 to CO and CH_4 in 0.1M NaOH solution with the TiO_2 and nanocomposites with different proportions of MgO, 1, 2 and 5% after 24 h reaction.

In addition to the products obtained in the gas phase, two products were detected in the liquid phase (Table 1), namely formic acid (HCOOH) and acetic acid (CH₃COOH). We can observe that the trend of photoactivity for CO_2 conversion for HCOOH and CH_3COOH was similar to the results in the gas phase, where the nanocomposite containing 1% of MgO showed better performance. From this, we confirmed that smaller amounts of basic oxides on the surface of TiO_2 are more effective for CO_2 photoreduction. It is important to note that the formation of acetic acid requires eight electrons and eight protons $(2CO_2 + 8e^2 + 8H^+ \rightarrow CH_3COOH)$, as well as for the production of methane, unlike the formic acid, which in turn requires two protons and two electrons $(CO_2 + 2e^2 + 2H^+ \rightarrow HCOOH)$ [1,2,37]. In addition, HCOOH is one of the intermediates in the production of CO [10] that also infers that this intermediate is rapidly consumed in successive reactions for the consequent production of CO.

Table 1. Amounts of HCOOH, CH₃COOH, CH₄ and CO formed after 24 h of CO₂ photoreduction catalyzed by the as-synthesized samples in the NaOH- solution and CH₄/CO ratio.

Samples	НСООН*	CH₃COOH*	CH ₄ *	CO*	CH ₄ /CO ratio (%)
TiO ₂	6.3	3.9	24.5	107.6	22.77
TiO ₂ /MgO – 1%	19.5	24.9	34.5	70.7	48.80
$TiO_2/MgO - 2\%$	6.8	7.3	20.3	100.4	20.22
$TiO_2/MgO - 5\%$	3.3	6.9	14.6	70.3	20.77

*µmol L⁻¹ g⁻¹

Several studies in the literature demonstrate that CO is one of the main intermediates in CH₄ formation, as discussed in the manuscript [38-40]. During CO production only two electrons are required, unlike CH₄ that needs eight electrons. Thus, we noticed that CH₄ production, in any condition, is very below the CO production, as also observed for the production of acetic acid, which, similar to methane, requires eight electrons for its production $(2CO_2 + 8e^- + 8H^+ \rightarrow CH_3COOH)$. Therefore, based on the results exhibited, we propose that products such as methane (CH₄) and acetic acid (CH₃COOH) are more difficult to form in this system since they need more electrons.

As discussed above, the formation of CH₄ can follow two main pathways, one having CO as intermediate (CO + e- \rightarrow C $^{\bullet}$ + H $^{\bullet}$ \rightarrow CH₃ $^{\bullet}$ + H $^{\bullet}$ \rightarrow CH₄), and the other by direct reduction of CO₂ (CO₂ + 8H $^{+}$ + 8e $^{-}$ \rightarrow CH₄ + 2H₂O). Thus, the higher CH₄/CO ratio presented by the TiO₂/MgO 1% (49.80%) sample may be related to the formation of CH₄ by the direct reduction of CO₂. On the other hand, the other samples have practically the same CH₄/CO ratio (~20%), as seen in Table 1, suggesting that the production of CH₄ by them preferably passes through the formed CO.

Another important aspect in the process of CO₂ photoreduction is the surface potential of the semiconductor as it relates to its stability in the aqueous suspension. The zeta potential of TiO₂ and TiO₂/MgO 1% decreased considerably with the increasing pH of the suspension, while the isoelectric point was 3.01 and 3.56, respectively (Fig. S4). At the point of zero charge, the particle surface is neutral which favors its aggregation in suspension. However, as the CO₂ photoreaction reactions were conducted at a higher pH than the isoelectric point, this medium favored its dispersion in the solution.

Also, as the TiO₂ has the isoelectric point at 3.01 and since the reaction is performed in NaOH solution (pH 6.4) the catalyst has a predominantly negative surface, which does not favor CO₂ adsorption. In addition, according to the equilibrium diagram of CO₂ in water [41], HCO₃ prevails in equilibrium at this pH. However, MgO has

isoelectric point at 10.0 [42], therefore the surface charge of MgO sites is positive. This favors the adsorption of HCO₃⁻ species, consequently increasing their activity in the CO₂ photoreduction process by contact.

Diffuse reflectance spectroscopy in the infrared region with a Fourier transform of the adsorbed CO_2 (DRIFTS- CO_2) was associated with the desorption technique with N_2 , while a flow purge was performed and the results obtained confirm what was previously discussed. The spectra obtained for TiO_2 and TiO_2/MgO 1% are similar, with band characteristic of carbonate (CO_3^{-2} : 1319, 1363, 1378, 1520 and 1522 cm⁻¹) [12] and bicarbonate (HCO_3^{-1} : 1228, 1448, 1626, 1650, 1682 cm⁻¹) [9,12,43,44] species adsorbed on the surface of these materials when subjected to CO_2 flow (Fig. 8).

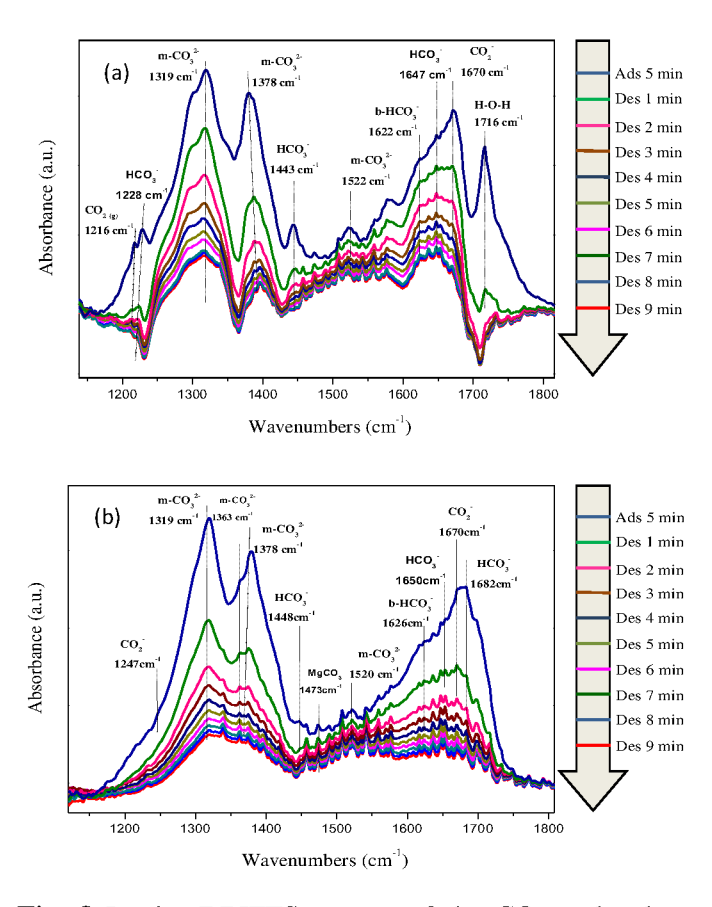


Fig. 8 In situ DRIFTS spectra of the CO₂ molecules adsorbed on (a) TiO₂ and (b) TiO₂/MgO 1%.

Species of type HCO₃⁻ produced by the CO₂ reaction with superficial OH groups [18] are possible intermediates in CO formation [9], and it is noteworthy that these species are better seen in TiO₂, especially in 1228 cm⁻¹ and 1443 cm⁻¹ (Fig. 8a). The presence of MgO on the surface of TiO₂ in TiO₂/MgO intensifies the adsorption process of CO₂

molecules by their basic character. MgO may bind to CO₂ to form Mg carbonate species [45], which is possible in a small amount, as suggested by a small peak at 1473 cm⁻¹ related to MgCO₃ (Fig. 8b). Although the mechanism of CO₂ photoreduction has not yet been fully clarified, it is known that the first step of the process may be the formation of the CO₂ anion by electrons originated from the defective surface of the semiconductor [16,37], evinced at 1670 cm⁻¹ in both semiconductors. These species are rapidly formed and gradually diminish over time [32]. However, for MgO-decorated material, the HCO₃ adsorption, is much more expressive, as seen by the peak at 1682 cm⁻¹ (Fig. 8b), suggesting that the CO₂ coordination is performed in hydrated form (carbonate anion). When the CO₂ flux is interrupted and N₂ introduced, the adsorbed species are rapidly desorbed, as shown Fig. 8., indicating a process of physisorption of the different species at the surface of the materials. This is an advantage from the point of view of catalysis, as reaction intermediates are produced and quickly desorbed, preventing the blocking of reaction sites. However, again, HCO₃ species are more persistent in the MgO-decorated sample, suggesting this coordination path. The peak at 1716 cm⁻¹ (Fig. 8a) is characteristic of H-O-H bending vibration band [46] of water molecules that may have adsorbed on the surface of TiO₂.

In addition to CO₂ adsorption, the desorption process in N₂ atmosphere was also analyzed (Fig. 9). As is well known, CO₂ is an acidic molecule and MgO in nanocomposite could irreversibly react, forming MgCO₃, ceasing any catalytic process [11,43,47]. However, desorption profiles (Fig. 9) suggest that CO₂ adsorption is reversible, despite being favored by MgO decoration: after two minutes of CO₂ flow, there is saturation of this gas, as can be observed in the spectrum at 2349 and 2370 cm⁻¹. In one minute (2340 and 2360 cm⁻¹), it is clear that the adsorption of CO₂ is preferential on the surface of TiO₂/MgO 1% compared to pure TiO₂, confirming that the presence of MgO favors the process of CO₂ adsorption. As the adsorption is favored by the presence of MgO, in the desorption process, CO₂ remains longer on the TiO₂/MgO 1% surface, i.e., the desorption is slower in this material despite taking place, as desired.

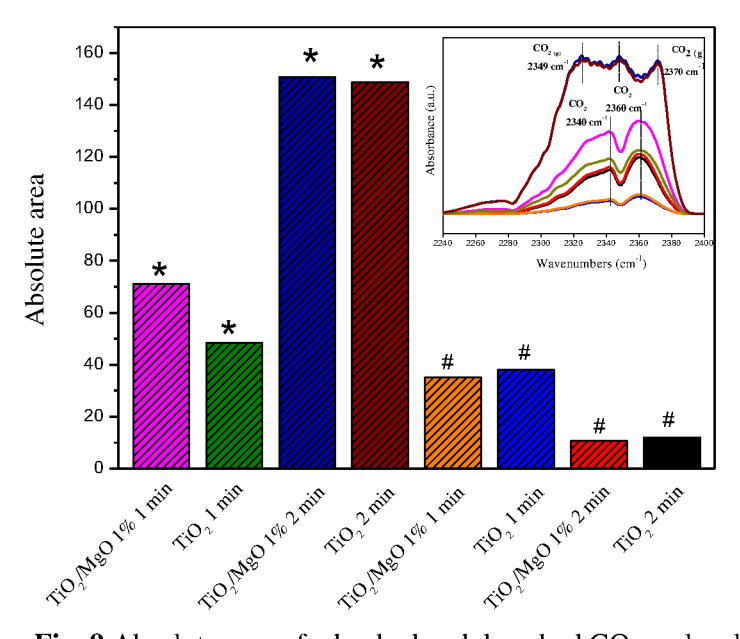


Fig. 9 Absolute area of adsorbed and desorbed CO_2 molecules on TiO_2 and TiO_2/MgO 1% at different times under N_2 flow (*adsorbed molecules and #desorbed molecules). Inset graph: In situ DRIFTS spectra.

3. Conclusions

In summary, we have shown how basic metal oxides such as MgO positively influence the catalytic activity of nanocomposites for CH₄ production by CO₂ photoreduction. This effect is only observed in small amounts of MgO, while in large amounts the insulating character of this oxide prevails, reducing the performance of semiconductors. The CO₂ photoreduction by TiO₂/MgO nanocomposites formed in the gaseous phase CH₄ and CO, suggesting that the production of the latter has CO as the intermediary, while the HCOOH and CH₃COOH were formed in the liquid phase. The high performance of these materials justifies their application to this proposal; however, it should be further explored for a better understanding of all the mechanisms involved.

Conflicts of interest

There are no conflicts to declare.

Acknowledgements

The authors are grateful to the Ministry of Science, Technology, and Innovation (through SisNANO Program – National System of Laboratories in

Nanotechnology), the National Council for Scientific and Technological Development (CNPq, Brazil China Virtual Center in Nanotechnology Project and grant #402.287/2013-4), Coordination for the Improvement of Higher Education Personnel (CAPES - Finance Code 001), Sao Paulo Research Foundation (FAPESP grants #15/14330-8, #16/21515-7), and Embrapa Rede AgroNano for their financial support. We thank the Brazilian Nanotechnology Laboratory for Research in Energy and Materials (LNNano) and the Structural Characterization Laboratory (LCE) for technical support during the X-ray photoelectron spectroscopy (grant #13839) and transmission electron microscopy experiments, respectively.

Caue Ribeiro also acknowledges Chinese Academy of Sciences (CAS) President's International Fellowship Initiative (PIFI) by financial support and CAPES – Alexander von Humboldt Foundation (Experienced Researchers Fellowship, CAPES Finance Code 001 – CAPES Process 88881.145566/2017-1).

References

- [1] S. S. Meryem, S. Nasreen, M. Siddique, R. Khan. An overview of the reaction conditions for an efficient photoconversion of CO₂. *Rev Chem Eng.*, **2017**, 34, 409-425.
- [2] X. Sun, Q. Zhu, X. Kang, H. Liu, Q. Qian, J. Ma, Z. Zhang, G. Yang, B. Han. Design of Cu (1)/C-doped boron nitride electrocatalyst for efficient conversion of CO₂ into acetic acid. *Green Chem.*, **2017**, 19, 2086-2091.
- [3] A. Crake, K. C. Christoforidis, A. Kafizas, S. Zafeiratos, C. Petit. CO₂ capture and photocatalytic reduction using bifunctional TiO₂/MOF nanocomposites under UV–vis irradiation. *Appl. Catal.*, *B*, **2017**, 210, 131-140.
- [4] S. Ijaz, M. F. Ehsan, M. N. Ashiq, N. Karamt, M. Najam-ul-Haq, T. He. Flower-like CdS/CdV₂O₆ composite for visible-light photoconversion of CO₂ into CH₄. *Mater. Des.*, **2016**, 107, 178-186.
- [5] M. F. Ehsan, R. Khan, T. He. Visible-Light Photoreduction of CO₂ to CH₄ over ZnTe-Modified TiO₂ Coral-Like Nanostructures. *ChemPhysChem*, **2017**, 18, 3203-3210.
- [6] Q. Guo, Q. Zhang, H. Wang, Z. Liu, Z. Zhao. Unraveling the role of surface property in the photoreduction performance of CO₂ and H₂O catalyzed by the modified ZnO. *J. Mol. Catal.*, **2017**, 436, 19-28.
- [7] L. Lin, C. Hou, X. Zhang, Y. Wang, Y. Chen, T. He. Highly efficient visible-light driven photocatalytic reduction of CO₂ over g-C₃N₄ nanosheets/tetra(4-carboxyphenyl) porphyrin iron(III) chloride heterogeneous catalysts. *Appl. Catal. B*, **2018**, 221, 312-319.
- [8] B. Selvaratnam, R. T. Koodali. TiO₂ -MgO mixed oxide nanomaterials for solar energy conversion. *Catal Today*, **2018**, 300, 39-49.
- [9] L. Liu, C. Zhao, H. Zhao, D. Pitts, Y. Li. Porous microspheres of MgO-patched TiO₂ for CO₂ photoreduction with H₂O vapor: temperature-dependent activity and stability. *Chem. Commun.*, **2013**, 49, 3664-3666.
- [10] L. Yuan, Y. J. Xu. Photocatalytic conversion of CO₂ into value-added and renewable fuels. *Appl. Surf. Sci.*, **2015**, 342, 54-167.
- [11] V. Hiremath, R. Shavi, J. G. Seo. Controlled oxidation state of Ti in MgO-TiO₂ composite for CO₂ capture. *Chem. Eng. J.*, **2017**, 308, 177-183.
- [12] Y. D. Ding, G. Song, Q. Liao, X. Zhu, R. Chen. Bench scale study of CO₂ adsorption performance of MgO in the presence of water vapor. *Energy*, **2016**, 112, 101-110.
- [13] N. C. Vega, O. Marin, E. Tosi, G. Grinblat, E. Mosquera, M. S. Moreno, M. Tirado, D. Comedi. The shell effect on the room temperature photoluminescence from ZnO/MgO core/shell nanowires: exciton–phonon coupling and strain. *Nanotechnol.*, **2017**, 28, 275702.
- [14] N. S. Allen, N. Mahdjoub, V. Vishnyakov, P. J. Kelly, R. J. Kriek. The effect of crystalline phase (anatase, brookite and rutile) and size on the photocatalytic activity of calcined polymorphic titanium dioxide (TiO₂). *Polym. Degrad. Stab.*, **2018**, 150, 31-36.
- [15] W. Tu, Y. Xu, J. Wang, B. Zhang, T. Zhou, S. Yin, S. Wu, C. Li, Y. Huang, Y. Zhou, Z. Zou, J. Robertson, M. Kraft, R. Xu. Investigating the role of Tunable Nitrogen Vacancies in Graphitic Carbon Nitride Nanosheets for Efficient Visible-Light-Driven H₂ evolution and CO₂ reduction. *ACS Sustainable Chem. Eng.*, **2017**, 58, 7260-7268.
- [16] W. Tu, Y. Zhou, Z. Zou. Photocatalytic Conversion of CO₂ into Renewable Hydrocarbon Fuels: State-of-the-Art Accomplishment, Challenges, and Prospects. *Adv. Mater.*, **2014**, 26, 4607-4626.
- [17] W. Tu, Y. Li, L. Kuai, Y. Zhou, Q. Xu, H. Li, X. Wang, M. Xiao, Z. Zou. Construction of unique two-dimensional MoS₂–TiO₂ hybrid nanojunctions: MoS₂ as a promising cost-effective cocatalyst toward improved photocatalytic reduction of CO₂ to methanol. *Nanoscale*, **2017**, 9, 9065-9070.
- [18] N. Abas, N. Khan. Carbon conundrum, climate change, CO₂ capture and consumptions. *J. CO₂ Util.*, **2014**, 8, 39-48.
- [19] M. Bellardita, A. D. Paola, B. Megna, L. Palmisano. Absolute crystallinity and photocatalytic activity of brookite TiO₂ samples. *Appl. Catal.*, *B*, **2017**, 201, 150-158.
- [20] V. Hiremath, M. L. T. Trivino, J. G. Seo. Eutectic mixture promoted CO₂ sorption on MgO-TiO₂ composite at elevated temperature. *J. Environ. Sci.*, **2019**, 76, 80-88.

- [21] X. Feng, F. Pan, H. Zhao, W. Deng, P. Zhang, H. Zhou, Y. Li. Atomic layer deposition enabled MgO surface coating on porous TiO₂ for improved CO₂ photoreduction. *Appl. Catal. B*, **2018**, 238, 274-283.
- [22] R. M. Mohamed, A. Shawky, I. A. Mkhalid. Facile synthesis of MgO and Ni-MgO nanostructures with enhanced adsorption of methyl blue dye. *J. Phys. Chem. Solids.*, **2017**, 101, 50-57.
- [23] H. W. Cho, K. L. Liao, J. S. Yang, J. J. Wu. Revelation of rutile phase by Raman scattering for enhanced photoelectrochemical performance of hydrothermally-grown anatase TiO₂ film. *Appl. Surf. Sci.*, **2018**, 440, 125-132.
- [24] D. Ortegadaz-Díaz, D. Fernández, S. Sepúlveda, R. R. Lindeke, J. J. Pérez-Bueno, E. Peláez-Abellán, J. Manríquez. Preparation of nanoparticulate TiO₂ containing nanocrystalline phases of anatase and brookite by electrochemical dissolution of remelted titanium components. *Arabian J. Chem.*, **2018**, In press.
- [25] O. F. Lopes, K. T. G. Carvalho, A. E. Nogueira, W. Avansi Jr, C. Ribeiro. Controlled Synthesis of BiVO₄ Photocatalysts: Evidence of the Role of Heterojunctions in their Catalytic Performance Driven by Visible-Light. *Appl. Catal.*, *B*, **2016**, 188, 87-97.
- [26] A. E. Nogueira, O. F. Lopes, A. B. S. Neto, C. Ribeiro. Enhanced Cr(VI) photoreduction in aqueous solution using Nb_2O_5/CuO heterostructures under UV and visible irradiation. *Chem. Eng. J.*, **2017**, 312, 220-227.
- [27] S. Ardizzone, C. L. Bianchi, M. Fadoni, B. Vercelli. Magnesium salts and oxide: an XPS overview. *Appl. Surf. Sci.*, **1997**, 119, 253-259.
- [28] F. Khairallah, A. Glisenti. XPS Study of MgO Nanopowders Obtained by Different Preparation Procedures. *Surf. Sci. Spectra*, **2007**, 13, 58.
- [29] B. A. Taleatu, E. Omotoso, C. Lal, W. O. Makinde, K. T. Ogundele, E. Ajenifuja, A. R. Lasisi, M. A. Eleruja, G. T. Mola. XPS and some surface characterizations of electrodeposited MgO nanostructure. *Surf. Interface Anal.*, **2014**, 46, 372-377.
- [30] S. Burnside, J.-E. Moser, K. Brooks, M. Gra1tzel. Nanocrystalline Mesoporous Strontium Titanate as Photoelectrode Material for Photosensitized Solar Devices: Increasing Photovoltage through Flatband Potential Engineering. *J. Phys. Chem. B.*, **1999**, 103, 9328-9332.
- [31] G. T. S. T. da Silva, A. E. Nogueira, J. A. Oliveira, J. A. Torres, O. F. Lopes, C. Ribeiro. Acidic surface niobium pentoxide is catalytic active for CO₂ photoreduction. *Appl. Catal. B.*, **2019**, 242, 349-357.
- [32] L. Liu, Y. Li. Understanding the Reaction Mechanism of Photocatalytic Reduction of CO₂ with H₂O on TiO₂ -Based Photocatalysts: A Review. *Aerosol Air Qual. Res.*, **2014**, 14, 453-469.
- [33] J. Kou, C. Lu, J. Wang, Y. Chen, Z. Xu, R.S. Varma. Selectivity Enhancement in Heterogeneous Photocatalytic Transformations. *Chem. Rev.*, **2017**, 117, 1445-1514.
- [34] J.-P. Jones, G.K.S. Prakash, G.A. Olah. Electrochemical CO₂ Reduction: Recent Advances and Current Trends. *Isr. J. Chem.*, **2014**, 54, 1451-1466.
- [35] S. R. Lingampalli, M. M. Ayyub, C. N. R. Rao. Recent Progress in the Photocatalytic Reduction of Carbon Dioxide. *ACS Omega.*, **2017**, 2, 2740-2748.
- [36] S. Sorcar, Y. Hwang, J. Lee, H. Kim, K. M. Grimes, C. A. Grimes, J.-W., Jung, C.-H. Cho, T. Majima, M. R. Hoffmann, S.-I. In. CO₂, water, and sunlight to hydrocarbon fuels: a sustained sunlight to fuel (Joule-to-Joule) photoconversion efficiency of 1%. *Energy Environ. Sci.*, **2019**, 1754-5692.
- [37] C. Genovese, C. Ampelli, S. Perathoner, G. Centi. Mechanism of C-C bond formation in the electrocatalytic reduction of CO_2 to acetic acid. A challenging reaction to use renewable energy with chemistry. *Green Chem.*, **2017**, 19, 2406-2415.
- [38] E. Karamian, S. Sharifnia. On the general mechanism of photocatalytic reduction of CO₂. *J. CO*₂ *Util.*, **2016**, 16, 194-203.
- [39] X. Chang, T. Wang, J. Gong. CO₂ photo-reduction: Insights into CO₂ activation and reaction on surfaces of photocatalysts. *Energy Environ. Sci.*, **2016**, 9, 2177-2196.
- [40] D. Ren, J. Fong, B.S. Yeo. The effects of currents and potentials on the selectivities of copper toward carbon dioxide electroreduction. *Nat. Commun.*, **2018**, 9, 1-8.

- [41] S. Lee, J. D. Ocon, Y. Son, J. Lee. Alkaline CO₂ Electrolysis toward Selective and Continuous HCOO⁻ Production over SnO₂ Nanocatalysts. *J. Phys. Chem. C*, **2015**, 119, 4884–4890.
- [42] B. Wang, X. Xiong, H. Rena, Z. Huang. Preparation of MgO nanocrystals and catalytic mechanism on phenol ozonation. *RSC Adv.*, **2017**, 7, 43464.
- [43] C. Xin, M. Hu, K. Wang, X. Wang. Significant Enhancement of Photocatalytic Reduction of CO₂ with H₂O over ZnO by the Formation of Basic Zinc Carbonate. *Langmuir*, **2017**, 33, 6667-6676.
- [44] A. Solis-Garcia, J. F. Louvier-Hernandez, A. Imendarez-Camarillo, J. C. Fierro-Gonzalez. Participation of surface bicarbonate, formate and methoxy species in the carbon dioxide methanation catalyzed by ZrO₂-supported Ni. *Appl. Catal.*, *B*, **2017**, 218, 611-620.
- [45] H. Abdullah, Md. M. R. Khan, H. R. Ong, Z. Yaakob. Modified TiO₂ photocatalyst for CO₂ photocatalytic reduction: An overview. *J. CO₂ Util.*, **2017**, 22, 15-32.
- [46] J. Singh, R. L. White. A variable temperature infrared spectroscopy study of CaA zeolite dehydration and carbonate formation. *Spectrochim. Acta, Part A*, **2019**, 207, 189-196.
- [47] Y. Yu, Y. M. Chan, Z. Bian, F. Song, J. Wang, Q. Zhong, S. Kawi. Enhanced performance and selectivity of CO₂ methanation over g-C₃N₄ assisted synthesis of Ni-CeO₂ catalyst: Kinetics and DRIFTS studies. *Int. J. Hydrogen Energy*, **2018**, 43, 15191-15204.